

A Conserved Hydrophobic Core in $G\alpha_{i1}$ Regulates G Protein Activation and Release from Activated Receptor*

Received for publication, June 27, 2016, and in revised form, July 25, 2016. Published, JBC Papers in Press, July 26, 2016, DOI 10.1074/jbc.M116.745513

Ali I. Kaya[‡], Alyssa D. Lokits[§], James A. Gilbert[‡], T. M. Iverson^{†¶}, Jens Meiler^{¶||}, and Heidi E. Hamm^{†¶1}

From the Departments of [‡]Pharmacology, [§]Neuroscience, [¶]Biochemistry, and ^{||}Chemistry, Vanderbilt University Medical Center, Nashville, Tennessee 37232

G protein-coupled receptor-mediated heterotrimeric G protein activation is a major mode of signal transduction in the cell. Previously, we and other groups reported that the $\alpha 5$ helix of $G\alpha_{i1}$, especially the hydrophobic interactions in this region, plays a key role during nucleotide release and G protein activation. To further investigate the effect of this hydrophobic core, we disrupted it in $G\alpha_{i1}$ by inserting 4 alanine amino acids into the $\alpha 5$ helix between residues Gln³³³ and Phe³³⁴ (Ins4A). This extends the length of the $\alpha 5$ helix without disturbing the $\beta 6$ - $\alpha 5$ loop interactions. This mutant has high basal nucleotide exchange activity yet no receptor-mediated activation of nucleotide exchange. By using structural approaches, we show that this mutant loses critical hydrophobic interactions, leading to significant rearrangements of side chain residues His⁵⁷, Phe¹⁸⁹, Phe¹⁹¹, and Phe³³⁶; it also disturbs the rotation of the $\alpha 5$ helix and the π - π interaction between His⁵⁷ and Phe¹⁸⁹. In addition, the insertion mutant abolishes G protein release from the activated receptor after nucleotide binding. Our biochemical and computational data indicate that the interactions between $\alpha 5$, $\alpha 1$, and $\beta 2$ - $\beta 3$ are not only vital for GDP release during G protein activation, but they are also necessary for proper GTP binding (or GDP rebinding). Thus, our studies suggest that this hydrophobic interface is critical for accurate rearrangement of the $\alpha 5$ helix for G protein release from the receptor after GTP binding.

Heterotrimeric G proteins, composed of α , β , and γ subunits, act as a molecular switches that turn on intracellular signaling cascades in response to the activation of G protein-coupled receptors by extracellular stimuli. Therefore, G proteins have a critical role in many different cellular responses (1–6).

The $G\alpha$ subunit binds GDP and forms a tight complex with the $G\beta\gamma$ subunits. Activated G protein-coupled receptors can catalyze the exchange of GDP for GTP, which leads to the dissociation of the receptor-G protein complex into isolated

receptor and $G\alpha$ and $G\beta\gamma$ subunits. Both the $G\alpha$ and $G\beta\gamma$ subunits can then stimulate or inhibit downstream effectors. Signal propagation ceases after the $G\alpha$ subunit hydrolyzes GTP, returns to the inactive state, and rebinds to the $G\beta\gamma$ subunit, regenerating the GDP-bound heterotrimeric state.

Previous studies showed that the activated receptor directly interacts with the G protein by binding to the C-terminal $\alpha 5$ helix of $G\alpha$, inducing a rigid body rotation and translation that pull this helix into a hydrophobic pocket on the receptor (7, 8). This leads to the rearrangement of the interfaces between helices $\alpha 5$, $\alpha 1$, and the $\beta 2$ - $\beta 3$ strands and between $\alpha 5$ and the $\beta 6$ - $\alpha 5$ loop (1, 7, 9–11). Residue Phe³³⁶ in the $\alpha 5$ helix is highly conserved in small (12, 13) and large GTPases (14) in both the animal and plant kingdoms (15–18). Our *in silico* results predicted that Phe³³⁶ is the most energetically important residue both in maintaining the basal state and in promoting the receptor-bound conformation (6). Our proposed mechanism involves Phe³³⁶ acting as a relay to transmit conformational changes via strands $\beta 2$ and $\beta 3$ and helix $\alpha 1$ to the phosphate-binding loop (5, 6). These studies are supported by recently published computational studies (11, 19, 20). Another critical computational paper from Dror *et al.* (21) used molecular dynamic simulations to suggest that the key events in receptor-mediated G protein activation and GDP release are due to the structural rearrangements of the $\beta 6$ - $\alpha 5$ loop. This is one of the two identified signal transmission pathways from the receptor to the GDP binding site (21).

To critically examine the roles of these two possible routes of communication with the nucleotide binding site, we inserted a 4-amino acid linker into the $\alpha 5$ helix of $G\alpha_{i1}$ between residues Gln³³³ and Phe³³⁴. This insert should disrupt the hydrophobic core (Phe³³⁶, His⁵⁷, Phe¹⁸⁹, and Phe¹⁹¹) and mimic the receptor-bound state while leaving the $\beta 6$ - $\alpha 5$ loop interactions intact (Fig. 1, A and B). Mutant $G\alpha_{i1}$ subunits were analyzed for their ability to interact with light-activated rhodopsin (R^*) to exchange nucleotides in both the basal and receptor-bound states and for the structural changes mediated by this insertion. In this study, $G\alpha_{i1}$ was used to replace the visual G protein found in rods, $G\alpha_{t1}$. $G\alpha_{i1}$ shows very close homology with $G\alpha_{t1}$, is activated by rhodopsin as well as $G\alpha_{t1}$ (22), and is much more easily expressed in *Escherichia coli*.

Our findings support the role of the hydrophobic interaction between $\alpha 5$, the $\beta 2$ - $\beta 3$ strands, and the $\alpha 1$ helix during activation and nucleotide release. We also uncovered an unexpected

* Work in the authors' laboratories was supported in whole or in part by National Institutes of Health Grants RO1EY006062 (to H.E.H.), RO1GM120569 (to T.M.I.), and RO1GM080403 (to J.M.). The authors declare that they have no conflict of interest with the contents of this article. The content is solely the responsibility of the authors and does not necessarily represent the official views of the National Institutes of Health.

The atomic coordinates and structure factors (codes 5KDL and 5KDO) have been deposited in the Protein Data Bank (<http://www.pdb.org/>).

¹ To whom correspondence should be addressed: Dept. of Pharmacology, 442 Robinson Research Bldg., Vanderbilt University Medical Center, Nashville, TN 37232-6600. Tel.: 615-343-3533; Fax: 615-343-1084; E-mail: Heidi.hamm@vanderbilt.edu.

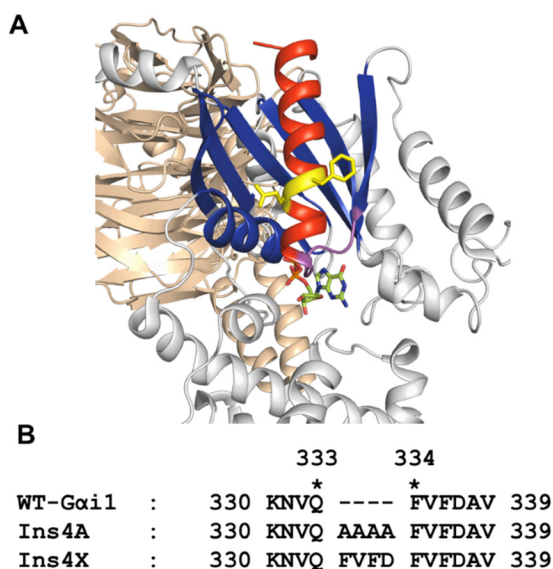


FIGURE 1. Heterotrimeric G protein; localization of 4-alanine insertion in $\alpha 5$ helix. *A*, ribbon representation of heterotrimeric G protein ($G_{\alpha}\beta\gamma$, PDB entry 1GP2 (24)). The G_{α} subunit is composed of nucleotide binding (blue) and helical (white) domains. The $\alpha 5$ helix (red) is a critical region for G protein stability and activation. This helix directly interacts with six β -strands ($\beta 1$ – $\beta 6$) and one α -helix ($\alpha 1$) (blue). Four amino acids were inserted between Gln³³³ and Phe³³⁴ (yellow) in the $\alpha 5$ helix. *B*, amino acid sequences and names of insertion mutants developed in this study.

dependence on these hydrophobic interactions for promoting G protein release from the receptor-G protein complex.

Results

Biochemical Characterization and Functional Properties of Ins4A-G α_{i1} Protein—To examine the two activation routes of G protein activation, we inserted 4 alanines between residues Gln³³³ and Phe³³⁴ of the $\alpha 5$ helix, with this variant termed Ins4A (Fig. 1, *A* and *B*). This insertion is proposed to perturb the interactions between the critical Phe³³⁶ and both the $\alpha 1$ helix and the $\beta 2$ - $\beta 3$ strands while leaving the $\beta 6$ - $\alpha 5$ loop intact. We tested how this insertion, which should mimic the rotation of the $\alpha 5$ helix toward the receptor in the R*-G $\alpha\beta\gamma$ complex, affects both the critical structural interactions between $\alpha 5$ and $\alpha 1$ and $\beta 1$ - $\beta 3$ and the functions of basal and receptor-mediated nucleotide exchange rates.

Ins4A displayed a highly increased basal exchange rate, as monitored by the relative increase in the intrinsic tryptophan (Trp²¹¹) fluorescence of G α_{i1} compared with WT protein (Fig. 2*A*, *light gray*). However, in receptor-mediated activation, the Ins4A mutant showed a significantly decreased nucleotide exchange rate compared with WT (*dark gray*).

One potential explanation for these data would be that the mutant does not interact with the receptor properly. To test this idea, we conducted a membrane binding assay with light-activated rhodopsin in rod outer segments (ROS).² The data show normal levels of Ins4A interaction with R* and the capability to bind ROS membrane as well as the WT protein (Fig.

2*B*). However, the addition of the GTP γ S non-hydrolyzable nucleotide analog does not induce disassociation of the complex even at high concentration (0.5 μ M) (Fig. 2*B*, *black arrows*). We repeated this experiment in the presence of 1 mM GDP, and once again, the mutant did not release from the ROS membrane. Densitometric calculations of membrane binding show that the mutant is not responsive to nucleotide (Fig. 2*C*).

Accordingly, an alternative possibility is that the Ins4A mutant might not properly dock its C terminus to R* to transmit the activation signal to the nucleotide binding region. Using extra-Meta II (eMII) to measure the high affinity state of the receptor shows that there is normal eMII induced by increasing concentrations of heterotrimeric G $_i$ binding (Fig. 2*D*), implying normal interaction between the $\alpha 5$ C-terminal helix and active receptor. Thus, the ability of G $_i$ to induce a high affinity state was similar between WT and Ins4A mutant (Fig. 2*D*). To confirm the nucleotide sensitivity in the membrane binding experiment (Fig. 2*B*), the eMII assay was repeated in the presence of a high concentration of GDP (0.5 mM). Even this high concentration of GDP did not inhibit eMII in Ins4A, although it did effectively inhibit it in the WT protein (compare Fig. 2, *D* and *E*). This result confirms the membrane binding results and also shows that the C terminus of Ins4A properly interacts with and induces the high affinity state of R* similar to WT.

Guanine Nucleotide Interactions with Ins4A Protein—There are several scenarios that might explain how the Ins4A protein could bind the receptor with similar affinity to WT yet lack receptor-mediated nucleotide exchange or nucleotide-dependent membrane release activity (Fig. 3*A*): 1) the helical domain opening does not take place properly, so GDP cannot release; 2) the $\beta 6$ - $\alpha 5$ loop does not properly trigger GDP release, as suggested by Dror *et al.* (21); 3) GDP can release normally, but GDP, GTP, or GTP γ S cannot rebind to the empty nucleotide-binding pocket; or 4) nucleotide exchange happens normally, but the G protein cannot release from the receptor.

To distinguish between these possibilities, we measured receptor-mediated GDP release and GTP γ S binding using BODIPY-labeled nucleotides. To measure GDP release from the G protein, the G α subunit was incubated with BODIPY-GDP, and then G $\beta\gamma$ was added as described under "Experimental Procedures." After 2 min, light-activated rhodopsin was added (Fig. 3*B*, *first arrow*). The data show that WT G $\alpha_{i1}\beta_1\gamma_1$ releases labeled GDP very quickly after interaction with R* (Fig. 3*B*, *black circles*), whereas Ins4A- $\beta_1\gamma_1$ releases GDP almost 100-fold more slowly (Fig. 3*B*, *gray trace*, and Table 2). The BODIPY-GDP dissociation rate constants were calculated to be ~ 3.52 and 0.042 min^{-1} for WT and the Ins4A mutant, respectively. To test whether GDP was still able to access the nucleotide binding region, we added excess unlabeled GDP and monitored BODIPY-GDP release. Unlabeled GDP can compete with the BODIPY nucleotide (Fig. 3*B*, *second arrow*). BODIPY-GDP release was faster in the presence of unlabeled GDP (dissociation rate, $\sim 0.755 \text{ min}^{-1}$); this is probably due to the affinity difference between these two GDP nucleotides.

GTP γ S binding was also monitored by using BODIPY-GTP γ S (Fig. 3*C*). Like GDP release, the Ins4A insertion mutant also affects GTP γ S binding. The data show that labeled GTP γ S interaction with the mutant was ~ 30 -fold slower than with the

² The abbreviations used are: ROS, rod outer segment(s); GTP γ S, guanosine 5'-[γ -thio]triphosphate; P-loop, phosphate binding loop; REU, Rosetta energy unit; eMII, extra-Meta II; β_2 AR, β_2 -adrenergic receptor; PDB, Protein Data Bank.

Structure of a $G\alpha$ C-terminal Insertion Mutant

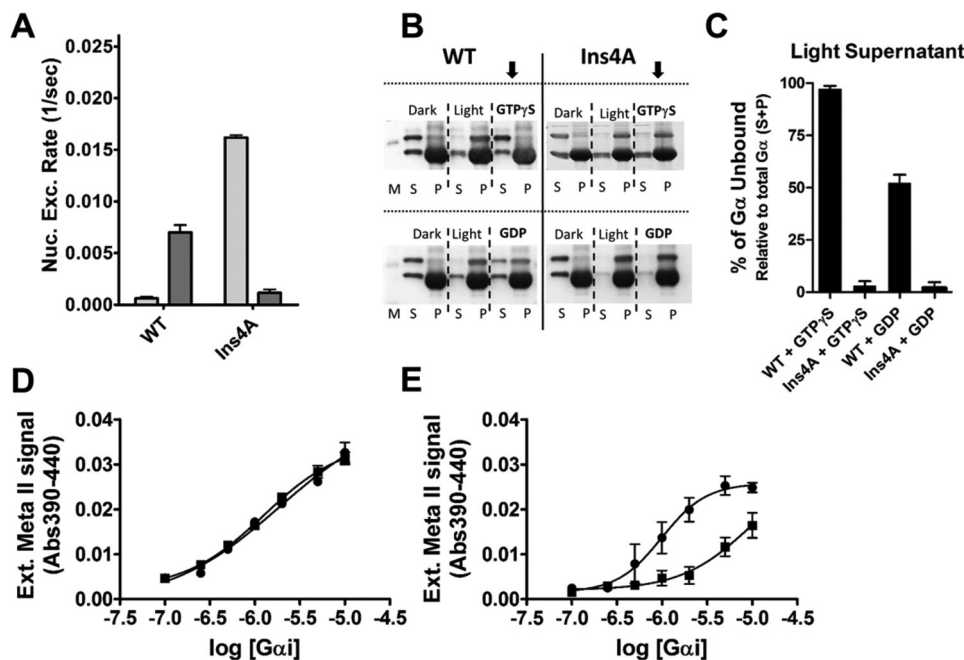


FIGURE 2. Biochemical properties of Ins4A protein. *A*, basal (gray bars) and receptor-mediated (dark gray bars) nucleotide exchange rates for wild type and 4-alanine insertion (Ins4A) mutations in $G\alpha_{i1}$ proteins. Nucleotide exchange was monitored by measuring the enhancement in intrinsic tryptophan (Trp^{211}) fluorescence ($\lambda_{\text{ex}} = 290 \text{ nm}$, $\lambda_{\text{em}} = 340 \text{ nm}$) as a function of time after the addition of $\text{GTP}\gamma\text{S}$ (32). The data were normalized to the baseline and maximum fluorescence and then fit to the exponential association equation ($y = y_{\text{max}} \times (1 - e^{-kt})$) to calculate the rate constant (k). Data were collected at 21 °C for 90 min. Results represent the mean \pm S.E. (error bars) values of at least three independent experiments. *B*, membrane binding of wild type and mutant $G\alpha_{i1}$ proteins. The assay was performed as described under "Experimental Procedures." *Dark*, from dark sample; *Light*, from light activated sample; *GTPγS* or *GDP*, from light-activated and nucleotide-incubated samples. *S*, supernatant; *P*, pellet. *C*, densitometric quantification of supernatant from light supernatant samples. Each sample from SDS-PAGE (*b*) was evaluated by comparison of the amount of $G\alpha_{i1}$ subunits in pellet (*P*) or supernatant (*S*) to the total amount of $G\alpha_{i1}$ subunits ($P + S$) in both treatments and expressed as a percentage of the total $G\alpha_{i1}$ protein. Data represent the average of three independent experiments. *D*, concentration-response curves of Meta-rhodopsin II (MII) signal stabilized by WT $G\alpha_{i1}$ (black square) and Ins4A (black circle). *E*, concentration-response curves of MII signal stabilized by WT $G\alpha_{i1}$ (black square) and Ins4A (black circle) in the presence of 0.5 mM GDP. The EC_{50} value of WT $G\alpha_{i1}$ and Ins4A protein for rhodopsin in ROS membranes was 9.43 ± 0.13 and $0.99 \pm 0.02 \mu\text{M}$, respectively. Solid curves are best fits from a four-parameter logistic equation. Results are mean \pm S.E. from of at least three independent experiments.

WT protein (Table 1); the binding rate reflects GDP release as well as labeled $\text{GTP}\gamma\text{S}$ interaction. The $\text{GTP}\gamma\text{S}$ binding rate constants were calculated to be 0.913 and 0.031 min^{-1} for WT and the Ins4A insertion mutant, respectively. These results indicate that the insertion of an extra helical turn in $\alpha 5$ dramatically affects receptor-mediated GDP release; however, GDP can still be released from the nucleotide binding pocket, and both GDP and $\text{GTP}\gamma\text{S}$ can access the pocket.

Examination of Conformational Changes in Functionally Important Regions Mediated by Receptor and $\text{GTP}\gamma\text{S}$ —To examine local environmental changes within specific regions of the $G\alpha$ subunit, we used a $G\alpha_{i1}$ protein lacking six solvent-exposed cysteines as a background for the introduction of cysteine residues at sites of interest. We selected three positions in the $G\alpha_{i1}$ subunit that are critical for G protein function (7). Leu^{273} (Leu^{296} in $G\alpha_s$) is a sensor of the presence of the guanine ring of guanine nucleotides, Lys^{349} (Arg^{389} in $G\alpha_s$) is a sensor of receptor binding, and Lys^{330} (Glu^{370} in $G\alpha_s$) senses rotation and disorder in $\alpha 5$ in the presence of R^* (8) (Fig. 4, *A* and *C*). These positions were mutated to Cys and labeled with the Alexa Fluor 594C5-maleimide probe. The fluorescent intensity was measured after a 40-min incubation with either GDP, $\text{GTP}\gamma\text{S}$, receptor, or receptor plus $\text{GTP}\gamma\text{S}$. Each result was normalized to the fluorescence of its wild type G protein (Fig. 4*D*, black bars). To determine the relative changes in those regions in the

basal state, we compared the fluorescence intensity in GDP- and $\text{GTP}\gamma\text{S}$ -bound states.

The -fold change in emission intensity of Ins4A in the presence of GDP (black bars) or $\text{GTP}\gamma\text{S}$ (gray bars) with the indicated labeled residues, as compared with the environment of the same labeled residue in WT are shown in Fig. 4*B*. The extreme C-terminal region (Lys^{349}) showed relatively low fluorescence intensity compared with the WT protein in both GDP and $\text{GTP}\gamma\text{S}$ bound states, which indicates a highly polar environment. This highly polar environment might be due to the more exposed location induced by the extra 4 alanine residues in the $\alpha 5$ helix. Other mutants were similar to WT.

Next, we evaluated the conformational changes of the same regions in the heterotrimeric G protein (black bars) in the presence of active receptor (gray bars) and after the addition of $\text{GTP}\gamma\text{S}$ (black shaded bars) (Fig. 4*D*). The decreased emission intensity from labeled Leu^{273} upon receptor activation indicates an increased polar environment for the probe in both WT and the insertion mutant, consistent with the effect of nucleotide release from the binding pocket after receptor interaction. After $\text{GTP}\gamma\text{S}$ incubation, the fluorescence intensity came back to its GDP bound level in both proteins, indicating nucleotide binding and domain closing.

Residue Lys^{330} is located at the beginning of the $\alpha 5$ helix; it senses rotation of the helix (7) and disorder in presence of active

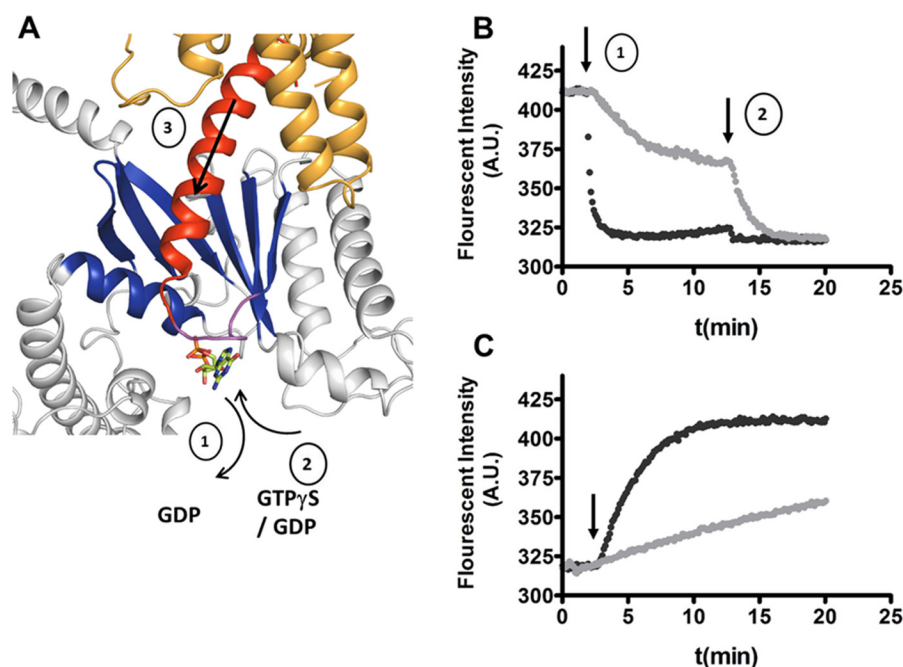


FIGURE 3. **Hypotheses for why Ins4A protein cannot release from the active receptor-G protein complex in presence of guanine nucleotide.** A, schematic representation of possible scenarios to explain biochemical data of the Ins4A proteins. 1, domain opening does not take place properly, so GDP cannot release or the domain is able to open, but the $\beta 6\alpha 5$ loop does not properly trigger GDP release. 2, GDP can release similar to WT $G\alpha_{11}$, but GDP, GTP, or $GTP\gamma S$ cannot bind the nucleotide binding pocket. 3, exchange of nucleotide happens normally, but the Ins4A protein cannot release from the receptor. B, BODIPY-GDP release from WT $G\alpha_{11}$ (black circle) and Ins4A (gray circle). The first and second arrows indicate the start of G protein incubation with light-activated rhodopsin and the addition of unlabeled GDP, respectively. C, BODIPY-GTP γS binding of WT $G\alpha_{11}$ (black circle) and Ins4A (gray circle). Arrow, the addition of light-activated rhodopsin. The fluorophore of BODIPY nucleotides was monitored at λ_{ex} 490 nm and λ_{em} 510 nm. The kinetic data were plotted and fit to a one-phase association function. Data are from a representative experiment that was repeated 8–10 times. A.U., arbitrary units.

TABLE 1
BODIPY nucleotide interactions with $G\alpha_{11}$

	BODIPY-GDP dissociation (k) \pm S.E.	BODIPY-GTP γS binding (k) \pm S.E.
	min^{-1}	
WT	3.521 ± 0.095	0.913 ± 0.045
Ins4A	0.042 ± 0.001	0.031 ± 0.007

receptor (8). The local environment of this residue indicated low solvent exposure in both WT and Ins4A after receptor interaction, indicating that it establishes new contact interactions that were absent in the heterotrimeric structure (Fig. 4D). These results are consistent with previous EPR studies (7). However, unlike WT, the mutant fluorescence intensity did not fully return to its heterotrimeric state after $GTP\gamma S$ incubation, indicating a perturbation in this region.

The extreme C terminus of $G\alpha$ is disordered or absent in most crystal structures of isolated $G\alpha$ or the $G\alpha\beta\gamma$ heterotrimer (23–26). It is a known receptor contact site that undergoes a receptor-mediated conformational change. Comparison of the fluorescence intensity of the Alexa Fluor label inserted in the C-terminal region at Lys³⁴⁹ in wild type *versus* the Ins4A- $G\alpha_{11}\beta_1\gamma_1$ suggests that this residue is in a similar environment before receptor activation. Upon binding to the light-activated rhodopsin, the \sim fold change in intensity indicates an immobilization of the probe for both wild type and Ins4A- $G\alpha_{11}\beta_1\gamma_1$, consistent with the expected interactions at the receptor-G protein interface (Fig. 4D, right). As expected, the strong fluorescence intensity of Lys³⁴⁹ disappeared in the $GTP\gamma S$ -bound WT G protein (Fig. 4D), whereas in the mutant, the signal did not

change, consistent with the membrane binding and eMII results (Fig. 2B).

Amino Acid Identity and the Hydrophobic Core Is Important for Rearrangement of the $\alpha 5$ Helix after Nucleotide Binding—To test whether the functional properties of the Ins4A protein are due to the longer $\alpha 5$ helix or due to disruption of the hydrophobic core, we replaced the 4-alanine insertion of Ins4A with a duplication of the 4 adjacent wild type residues (from Phe³³⁴ to Asp³³⁷), terming the variant Ins4X (Fig. 1B). This change reestablishes the hydrophobic core around Phe³³⁶ ($\alpha 5$) in the presence of an insertion while altering the length of $\alpha 5$ to be the same as Ins4A. To investigate the function of the Ins4X protein, we evaluated its nucleotide exchange rates and membrane binding properties. Unlike Ins4A, Ins4X exhibited basal and receptor-mediated nucleotide exchange rates (Fig. 5A) and membrane binding (Fig. 5B) similar to wild type $G\alpha_{11}\beta_1\gamma_1$. The Ins4X protein dissociated from ROS membrane after incubation with active receptor and $GTP\gamma S$, similar to WT (Fig. 2B). As shown in Fig. 5B, unlike Ins4A, Ins4X released from the ROS membrane completely after incubation with nucleotide. This result suggests that the effect of Ins4A on G protein function is not due to the increase in length of the C terminus. Instead, it suggests that the amino acid identity and the establishment of the hydrophobic core play critical roles for proper rearrangement of the $\alpha 5$ helix and $G\alpha$ subunit release from the receptor after nucleotide binding.

X-ray Structures of the Ins4A Mutant—To probe the structural basis for the biochemical properties of the Ins4A variant, the crystal structure in the $GTP\gamma S$ -bound state was determined

Structure of a $G\alpha$ C-terminal Insertion Mutant

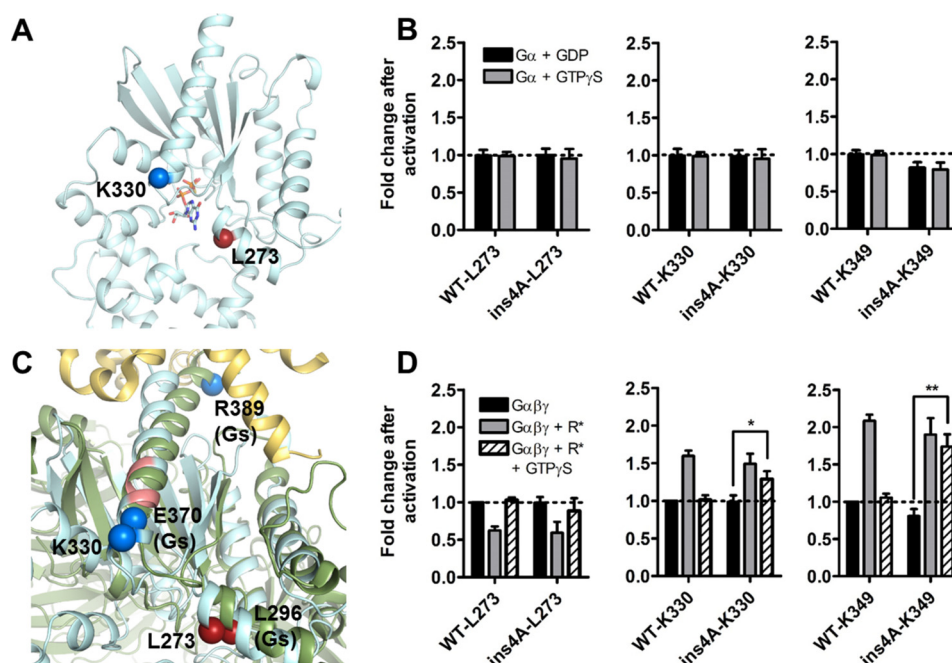


FIGURE 4. **Conformational changes at key sites on $G\alpha$ caused by receptor and $GTP\gamma S$ determined using site-directed fluorescent labels.** Leu²⁷³ (Leu²⁹⁶ in $G\alpha_s$) residue is a sensor of the presence of the guanine ring of GDP, Lys³⁴⁹ (Arg³⁸⁹ in $G\alpha_s$) is a sensor of receptor binding, and Lys³³⁰ (Glu³⁷⁰ in $G\alpha_s$) is a sensor of rotation and disorder in the presence of active receptor (32). *A*, schematic representation of labeled residues in the Ins4A- $G\alpha_{11}$ -GDP protein. *B*, -fold change in emission intensity of $G\alpha_{11}$ proteins in the presence of GDP (black bars) or $GTP\gamma S$ (gray bars) in the presence of the indicated labeled residues, as compared with the environment of the same labeled residue in the WT GDP-bound state. *C*, comparison of labeled residues between Ins4A (cyan) and β_2 adrenergic receptor- $G\alpha_s$ complex structure (PDB entry 3SN6 (8), green). *D*, -fold change emission intensity of $G\alpha_{11}\beta_1\gamma_1$ (black bars) in the presence or absence of light-activated rhodopsin (gray bars) and $GTP\gamma S$ (white bars). Data are the average of at least three independent experiments (*, $p < 0.05$; **, $p < 0.01$). Error bars, S.E.

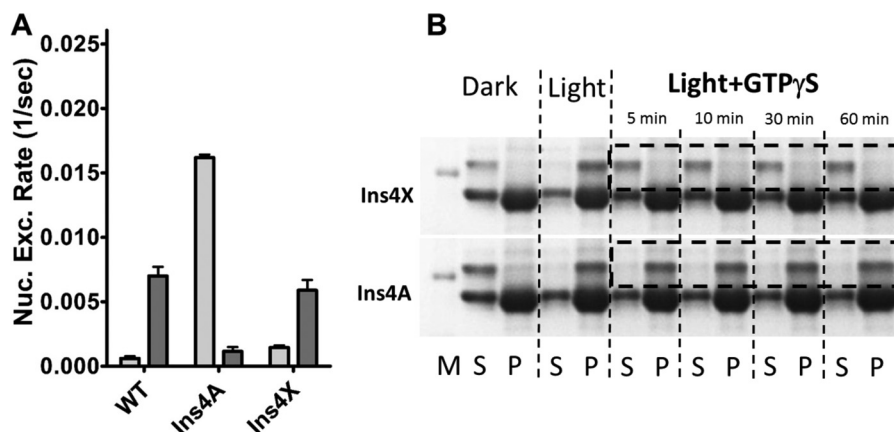


FIGURE 5. **The effect of introducing an FVFD insertion in the α_5 helix on $G\alpha_{11}$ subunit.** *A*, basal (gray bars) and receptor-mediated (dark gray bars) nucleotide exchange rates for WT, Ins4A, and FVFD insertion mutation (Ins4X) in $G\alpha_{11}$ proteins. Nucleotide exchange was monitored by measuring the enhancement in intrinsic tryptophan (Trp²¹¹) fluorescence as a function of time after the addition of $GTP\gamma S$ (32). Data were collected at 21 °C for 90 min and represent the mean \pm S.E. values of at least three independent experiments. *B*, membrane binding of Ins4A and Ins4X proteins. *Dark*, from dark sample; *Light*, from light activated sample; *GTP γ S* or *GDP*, from light-activated and nucleotide-incubated samples. *S*, supernatant; *P*, pellet. Data represent the average of three independent experiments. Error bars, S.E.

at 2.7 Å resolution (Table 2). After insertion of the 4 alanines between Gln³³³ and Phe³³⁴, the α_5 helix rotates $\sim 60^\circ$ starting from the insertion point (Fig. 6*A*, labeled in red). This rotation relocates Phe³³⁶ to a position similar to that observed for the homologous residue (Phe³⁷⁶) in the β_2 -adrenergic receptor (β_2 AR)- G_s complex structure (8) (Fig. 6*B*, compare WT $GTP\gamma S$ (brown), Ins4A (cyan), and β_2 AR- G_s (green) (PDB entry 3SN6 (8))). Although attempted, we could not crystallize either the GDP-bound or nucleotide-free Ins4A protein.

The 4-Ala insert completely repositions the network of interactions between Phe³³⁶ (α_5), Phe¹⁸⁹, Phe¹⁹¹, Phe¹⁹⁶ (β_2 - β_3),

and His⁵⁷ (α_1). It also disturbs the π - π interaction between His⁵⁷ and Phe¹⁸⁹ (Fig. 6, *C* and *D*). In Ins4A, almost the entire β_2 - β_3 strands move away from the α_5 helix compared with the WT structure (Fig. 6, *C* and *D*). The relative $C\alpha$ distances between insertion mutant and WT proteins in Phe¹⁸⁹, Phe¹⁹¹, Lys¹⁹², and Phe¹⁹⁶ are 1.5, 2.3, 3.8, and 1 Å, respectively, whereas the overall root mean square deviation between WT $G\alpha_{11}$ and Ins4A was 0.79 Å (304 $C\alpha$ atoms aligned totally).

Crystallized Ins4A has $GTP\gamma S$ bound, and the guanine nucleotide holds the GTPase and helical domains together in the structure. Therefore, we did not expect to see any signifi-

cant differences between the WT and mutant structure in the nucleotide contact regions. However, we identified an interesting feature in this structure. In the structure of Ins4A, the side chain of His⁵⁷ (localized on the end of the α 1 helix) flips from pointing inside to outside of the core, probably due to the lost network of interactions between Phe³³⁶ (α 5), Phe¹⁸⁹ (β 2), and

Phe¹⁹¹ (β 2). The relative C α distances in the α 1 helix for residues Ile⁵⁵, Ile⁵⁶, His⁵⁷, and Glu⁵⁸ are 0.5, 0.9, 1.3, and 1.2 Å, respectively, between the Ins4A insertion mutant and the WT protein, with the end of the α 1 helix moving away from α 5. This structural rearrangement of the end of the α 1 helix and His⁵⁷ were predicted in our Rho-G_i complex model (Fig. 6F, gray) (19). The β 2AR-G α_s complex structure (Fig. 6E), is lacking the end of the α 1 helix.

TABLE 2
Crystallographic data collection and refinement statistics

	Ins4A-G α i1-GTP γ S-Mg ²⁺	Ins4A-G α i1 β 1 γ 1-GDP
PDB accession code	5KDL	5KDO
Data Collection and Processing^a		
Beamline	21-ID-F	21-ID-G
Space groups	P2 ₁	P4 ₃
Cell Dimensions: a, b, c (Å)	61.7, 77.3, 73.1	84.65, 84.65, 130.09
α , β , γ (degrees)	90, 99.8, 90	90, 90, 90
Resolution (Å)	50.0-2.8 (2.8-2.7)	40.25-1.90 (1.97-1.90)
Total Reflections	217,114	1,504,669
Unique Reflections	19,135	71,960
R _{sym} ^b (%)	8.8 (51.7)	7.4 (123.4)
R _{rim} ^c (%)	5.6 (33.6)	4.3 (54.0)
$\langle I \rangle / \langle \sigma \rangle$	14.4 (2.04)	17.4 (1.4)
Completeness (%)	99.5 (97.4)	100 (100)
Refinement Statistics		
R _{work} ^d (%)	20.9	18.21
R _{free} (%)	26.4	20.79
RMS deviations		
Bond (Å)	0.002	0.007
Angle (°)	0.522	0.977
Ramachandran statistics^e		
Favored (%)	99.2	98.07
Allowed (%)	0.8	1.93
Outliers (%)	0.0	0.0

^aNumbers in parentheses indicate statistics for the highest shell.

^b $R_{sym} = \sum |I_i - \langle I \rangle| / \sum I_i$ where I is intensity, I_i is the i th measurement, and $\langle I \rangle$ is the weighted mean of I .

^c $R_{rim} = \sum_{hkl} \sqrt{[1/(N-1)] \sum_i |I_i(hkl) - \langle I(hkl) \rangle|} / \sum_{hkl} \sum_i I_i(hkl)$ where I is running over the number of independent observations of reflection hkl and N is representing the number of replicate observations.

^d $R_{work} = \sum ||Fo| - |Fc|| / \sum |Fo|$ where Fo and Fc are the observed and calculated structure factor amplitudes. R_{free} is the same as R_{work} for a set of data omitted from the refinement.

^eRamachandran analysis from MOLPROBITY (57).

Structural Features of the Ins4A- β 1 γ 1 Mutant—In the β 2AR-G_s complex crystal structure (8), the G β ₁ γ ₂ subunit does not make any contact with the receptor and does not undergo statistically significant conformational changes upon complex formation, although, because of the low resolution of that structure, some real changes might not have been statistically significant. To evaluate any possible role of the G β γ subunits in the biochemical properties seen in the Ins4A mutant, we determined the crystal structure of the heterotrimeric Ins4A- β 1 γ 1 mutant in the GDP-bound state to 1.9 Å resolution (Table 2 and Fig. 7A). The Ins4A- β 1 γ 1 structure shows a similar α 5 helix rotation pattern as the isolated Ins4A bound to GTP γ S (Fig. 7A, teal). However, there was no dramatic displacement of the α 1 helix and β 2- β 3 regions (Fig. 7A). The relative C α distances between mutant (Fig. 7A, teal) and WT (yellow) heterotrimeric structures in His⁵⁷, Phe¹⁸⁹, Phe¹⁹¹, Lys¹⁹², and Phe¹⁹⁶ residues are 0.5, 0.5, 1.4, 1.4, and 0.6 Å, respectively. This might be due to the effect of the crystal packing. Fig. 7, B and C, shows that the α 5 helix, β 2- β 3 strands, and α 1 helix interact with a symmetric molecule of the G β ₁ γ ₁ subunit, which might block or limit the displacement of the β 2- β 3 strands and α 1 helix. The Ins4A- β 1 γ 1 heterotrimeric structure also shows significant differences at the α N (Fig. 7D) and α 2 helices and the G β ₁ γ ₁ subunits (Fig. 7E) compared with the WT structure. There is not any

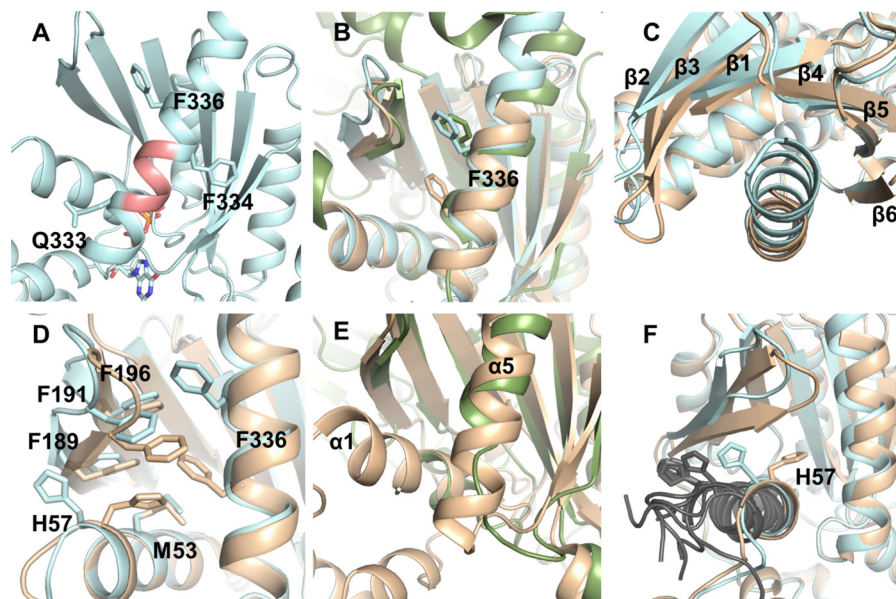


FIGURE 6. Structural features of GTP γ S-bound Ins4A mutant protein. A, schematic representation of Gln³³³, Phe³³⁴, and Phe³³⁶ residues in the α 5 helix of Ins4A. The 4-alanine insertion region is represented in salmon color. B, comparison of the α 5 helix and Phe³³⁶ residue location between WT G α_{i1} (PDB entry 1GIA (26), brown), Ins4A (cyan), and β 2AR-G α_s complex structure (PDB entry 3SN6 (8), green). C, comparison of the α 5 helix and β 1- β 6 strands between WT G α_{i1} (brown) and Ins4A (cyan). D, the effect of α 5 helix rotation and the connection between Phe³³⁶ and the β 2- β 3 strands and the α 1 helix. Shown is a comparison of α 5, β 2- β 3, and α 1 regions between WT G α_{i1} (brown) and Ins4A (cyan). This structure shows significant rearrangement of side chains in His⁵⁷, Phe¹⁸⁹, Phe¹⁹¹, and Phe¹⁹⁶ and disturbed π - π interaction between His⁵⁷ and Phe¹⁸⁹. E, comparison of β 2AR-G α_s complex structure (green) and WT G α_{i1} β ₁ γ ₂ (brown); F, relative position of residue His⁵⁷ and the α 1 helix between WT G α_{i1} (brown), Ins4A (cyan), and rhodopsin-G protein model (gray) (19).

Structure of a $G\alpha$ C-terminal Insertion Mutant

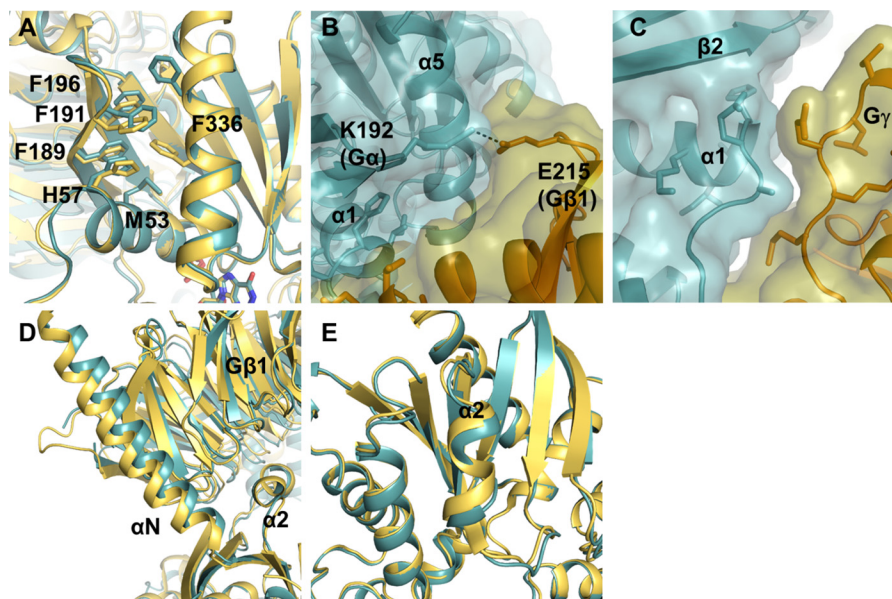


FIGURE 7. **Structural features of heterotrimeric Ins4A β 1 γ 1 mutant protein.** A, comparison of the α 5, β 2- β 3, and α 1 regions between WT $G\alpha_{i1}\beta_1\gamma_2$ (PDB entry 1GP2, yellow) and Ins4A β 1 γ 1 (teal). The relative $C\alpha$ distances between mutant and WT heterotrimeric structure protein in His⁵⁷, Phe¹⁸⁹, Phe¹⁹¹, Lys¹⁹², and Phe¹⁹⁶ are 0.5, 0.5, 1.4, 1.4, and 0.6 Å, respectively. B, the interaction between Lys¹⁹² in the $G\alpha$ subunit, the β 2- β 3 loop (teal), and Glu²¹⁵ in the $G\beta_1$ subunit in a symmetry molecule (orange). C, contact between the $G\alpha$ subunit α 1 helix and $G\gamma$ 1 in a symmetry molecule (orange). Shown is a surface representation in teal and orange for mutant and WT structures, respectively. D and E, comparison of the α N (D) and α 2 helices (E) between Ins4A β 1 γ 1 (teal) and WT $G\alpha_{i1}\beta_1\gamma_2$ (PDB entry 1GP2 (24), yellow) protein.

TABLE 3

G protein α subunit α 1 helix interface energetic predictions

Entity	Amino acid	Ins4A-GTP γ S		WT GTP γ S		Ins4A β 1 γ 1		WT β 1 γ 2	
		Energy	Z score	Energy	Z score	Energy	Z score	Energy	Z score
		REU		REU		REU		REU	
β 1	Leu ³⁸	1.1	75	1.2	281	1.4	53	2.0	17
P-loop	Gly ⁴⁰	0.8	103						
α 1	Lys ⁴⁶	1.3	53	1.1	89	1.9	6	1.9	35
α 1	Ser ⁴⁷	0.7	61						
α 1	Thr ⁴⁸	0.9	52	0.8	154	0.7	27	0.9	27
α 1	Ile ⁴⁹	1.0	38	1.0	179	1.1	192	1.0	10
α 1	Val ⁵⁰			0.5	235	0.9	118		
α 1	Gln ⁵²	1.2	25	1.5	34	1.7	266	1.6	25
α 1	Met ⁵³	0.5	6	1.4	462	1.0	116	1.4	14
α 1	Lys ⁵⁴	1.8	122	2.3	101	2.2	441	2.5	24
α 1	Ile ⁵⁵	1.4	170	1.0	263	1.0	158	1.0	10
α 1	Ile ⁵⁶	1.0	85	1.1	57			1.1	35
α 1	His ⁵⁷	1.3	28	1.6	133	1.5	127	1.7	34
Linker 1	Gly ⁶⁰			0.7	71	0.9	339	0.9	67
Linker 1	Tyr ⁶¹	1.0	125	1.5	70	0.8	208	1.0	9
α A	Glu ⁶⁵	0.8	104	0.5	9	0.8	384	0.8	52
α F	Leu ¹⁷⁵	0.9	51	1.0	279	1.0	104	1.0	23
β 2	Phe ¹⁸⁹	1.0	13	1.4	114	1.5	229	1.4	28
β 2	Phe ¹⁹¹								
β 3	Met ¹⁹⁸					0.5	73	0.5	6
β 3	Asp ²⁰⁰	0.8	84			1.0	3	1.0	24
β 6- α 5	Ala ³²⁶	1.3	53	1.3	88	1.3	124	1.6	38
β 6- α 5	Thr ³²⁹	0.5	21	0.8	100	0.8	346	0.8	16
α 5	Val ³³²	0.6	11	0.7	189	0.7	397	0.8	35
α 5	Phe ³³⁶			0.9	736			0.8	24

direct interaction between the 4-Ala insertion site and these regions. Therefore, these structural differences might be allosteric effects of the insertion region. Another possibility is that all three heterotrimeric structures, $G\alpha_i\beta_1\gamma_1$, $G\alpha_{i1}\beta_1\gamma_2$, and Ins4A- $G\alpha_{i1}\beta_1\gamma_1$, contain the same $G\beta$ and $G\gamma$ subtype combinations, which might affect the heterotrimeric structures in specific regions. The root mean square deviation of the $G\alpha$ subunit and heterotrimeric structure between WT β 1 γ 2 (PDB entity 1GP2 (24)) and Ins4A- β 1 γ 1 was 0.82 and 1.2 Å (with a total of 329 and 697 $C\alpha$ atoms aligned, respectively).

The Effect of the 4-Alanine Insertion on α 1 Helix Interface Binding Energy—To investigate the effect of the extra helical turn of α 5 on the α 1 helix computationally, we calculated inter-action energy scores for all residues within the α 1 helix in both the $G\alpha_{i1}$ monomer and heterotrimeric $G\alpha_{i1}\beta_1\gamma_1$ proteins using an established protocol (19) (Table 3). These $\Delta\Delta G$ values probed for a potential network of intramolecular interactions, which could propagate the conformational changes necessary for G protein activation and nucleotide exchange. The $\Delta\Delta G$ calculations predicted and support the crystallographic data.

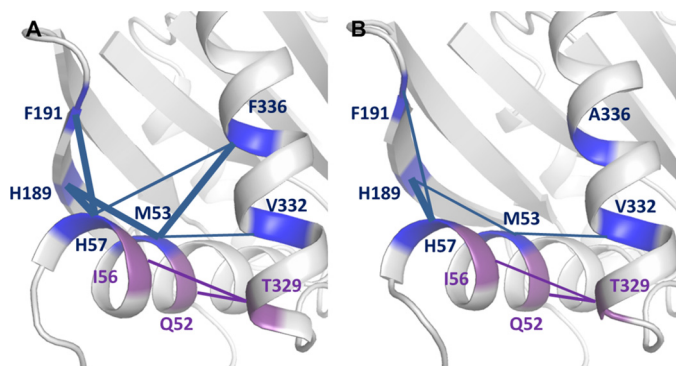


FIGURE 8. Pairwise interaction scores highlight two activation pathways. There are two critical stabilizing routes between the $\alpha 1$ and $\alpha 5$ helices in the GDP-bound state. The first (purple) is between Gln⁵² ($\alpha 1$), Ile⁵⁶ ($\alpha 1$), and Thr³²⁹ ($\alpha 5$). The second pathway (blue) connects Met⁵³ ($\alpha 1$), His⁵⁷ ($\alpha 1$), Val³³² ($\alpha 5$), and Phe³³⁶ ($\alpha 5$). A, WT $G\alpha_1$ (PDB entry 1GIA (26)) maintains both networks in the GDP-bound state. B, the Ins4A mutant loses the hydrophobic core between $\alpha 5$, $\alpha 1$, and the $\beta 2$ - $\beta 3$ strands.

We did not see any major differences at the N terminus of the $\alpha 1$ helix, Leu⁴⁶-Ile⁴⁹, compared with the WT protein structure. However, starting from Val⁵⁰, significant differences were identified between mutant and WT proteins. The predicted $\Delta\Delta G$ values of Gln⁵², Met⁵³, Ile⁵⁶ and His⁵⁷ residues, which play a major role in interaction with and stabilization of the $\alpha 5$ helix in the GDP-bound state, were decreased compared with WT (11, 19, 20, 27). The total interaction energy score was ~ 4 Rosetta energy units (REUs) in the Ins4A compared with 5.5 REUs in the WT protein (Table 3).

There are two critical stabilizing routes between the $\alpha 1$ and $\alpha 5$ helices in the GDP-bound state. To look at the individual residue-residue interactions and distinguish between these two pathways, we used Rosetta to predict the network energy scores between all amino acid pairs in our structural models and protein crystals. The first route is between Gln⁵² ($\alpha 1$) and Ile⁵⁶ ($\alpha 1$) with Thr³²⁹ ($\alpha 5$). Previously, Kapoor *et al.* (28) showed that the T329A mutation causes high $G\alpha_1$ activity. The pairwise interaction scores were calculated between Gln⁵² ($\alpha 1$) and Thr³²⁹ ($\alpha 5$) and between Ile⁵⁶ ($\alpha 1$) and Thr³²⁹ ($\alpha 5$) as 0.5 and 0.2 REUs, respectively. The second pathway is between Met⁵³ ($\alpha 1$) and His⁵⁷ ($\alpha 1$) with Val³³² ($\alpha 5$) and Phe³³⁶ ($\alpha 5$), a part of the hydrophobic core between $\alpha 5$, $\alpha 1$, and $\beta 2$ - $\beta 3$ strands (Fig. 8). The structural rearrangement at the end of the $\alpha 1$ helix also affects linker 1 and the beginning of the αA helix. The $\Delta\Delta G$ values calculated at Gly⁶⁰ (linker 1) decreased from 0.7 to under 0.5; at Tyr⁶¹, it was changed from 1.5 to 1.0 REU compared with WT protein. In Glu⁶⁵ (αA), it increased from 0.5 to 0.8 REUs, as it approached linker 1. In the heterotrimeric structures, we observed a similar pattern between Ins4A and WT but with smaller margins.

Discussion

Two receptor-mediated G protein activation routes have been hypothesized. In the first, binding of the receptor to the C terminus of $G\alpha$ is thought to trigger conformational changes that can be transmitted to the nucleotide-binding pocket via outward rotation and translation of the $\alpha 5$ helix and distortion of the $\beta 6$ - $\alpha 5$ loop, a key site of interaction with the guanine ring (8, 21, 29–31). In the second pathway, the receptor-dependent

$\alpha 5$ rotation and translation destabilizes the hydrophobic interactions between the $\alpha 5$ and $\alpha 1$ helices and the $\beta 2$ - $\beta 3$ strands, which weaken both phosphate and purine binding sites of nucleotide (10, 11, 20, 27, 28). In the two proposed activation pathways, the extreme C terminus of the $\alpha 5$ helix facilitates both receptor-G protein interaction and G protein activation (2, 8, 9, 32, 33). To separate these two pathways and to further investigate the effect of the hydrophobic core between $\alpha 5$, $\alpha 1$, and $\beta 2$ - $\beta 3$ strands, we inserted a 4-Ala linker between Gln³³³ and Phe³³⁴ in the $\alpha 5$ helix.

Our data show that the Ins4A mutant caused high basal nucleotide exchange, as anticipated from previous studies (9–11). The Ins4A-GTP γ S crystal structure showed that, starting from Gln³³³, the $\alpha 5$ helix is displaced by an extra helical turn, which partially mimics the effect of the receptor on the G protein. Indeed, Phe³³⁶ of the $\alpha 5$ helix, which we previously showed was a critical residue for forming a hydrophobic core in the $G\alpha$ subunit, is localized at a position similar to where it is localized in the $\beta 2AR$ -Gs complex structure.

The $\alpha 5$ helix is protected and surrounded with mostly hydrophobic interactions by six β -strands ($\beta 1$ – $\beta 6$) and one α helix ($\alpha 1$). The effects of $\alpha 5$ helix rotation on the β strands are clearly observed in the Ins4A structure compared with WT protein. The relative positions of the $\beta 5$ and $\beta 6$ strands are not affected by the rotation, and these two strands almost perfectly superimpose with the WT structure. However, there are significant and progressive differences in the β -strands N-terminal to $\beta 4$. This is most dramatically observed in the $\beta 2$ - $\beta 3$ strands. This rotation completely repositions the network of interactions between Phe³³⁶ ($\alpha 5$); Phe¹⁸⁹, Phe¹⁹¹, and Phe¹⁹⁶ ($\beta 2$ - $\beta 3$); and Met⁵³ and His⁵⁷ ($\alpha 1$), including disturbing the π - π interaction between His⁵⁷ and Phe¹⁸⁹. The conformational changes in this region mimic the receptor-bound state (10, 11, 20, 27, 34). This result supports the second route of G protein activation (see above), which was proposed in our previous study (11) and was recently supported by Flock *et al.* (20) and Sun *et al.* (27) via using evolutionary analysis and alanine scanning approaches, respectively.

In the $\beta 2AR$ - G_s complex structure, the $\alpha 1$ helix, starting from Met⁵³ (Met⁶⁰ in $G\alpha_s$), is not ordered (8). In the rhodopsin- G_i complex model, it was predicted that the end of the $\alpha 1$ helix would move away from $\alpha 5$, and most of the residues (from Gln⁵² to His⁵⁷) would lose contact with the $\alpha 5$ helix after GDP release and helical domain opening (19). The Ins4A mutant structure confirmed this prediction, although we could only crystallize the GTP γ S-bound state, which holds the GTPase and helical domains together. Given that it is GTP γ S-bound, significant differences between WT and mutant structures in the nucleotide contact regions, such as the P-loop and $\beta 6$ - $\alpha 5$ loop, were not expected. However, it appears that the reorganization between the $\alpha 5$ helix and $\beta 2$ - $\beta 3$ strands is enough to trigger the $\alpha 1$ rearrangement although the $\beta 6$ - $\alpha 5$ loop and first helical turn of the $\alpha 5$ helix are still intact.

In contrast to its high constitutive activity in the basal state, the Ins4A mutant showed very little receptor-mediated nucleotide exchange activity. This, we believe, is due to the effect of the $G\beta\gamma$ subunit. In the basal state, without $G\beta\gamma$, the $G\alpha$ subunit does not require a large displacement of $\alpha 5$ and the $\beta 6$ - $\alpha 5$

Structure of a $G\alpha$ C-terminal Insertion Mutant

loop to release GDP from the binding pocket. Perturbation of $\beta 2$ - $\beta 3$, $\alpha 1$, and the Mg^{+2} binding regions is sufficient to trigger GDP release (10, 11, 28). However, in the heterotrimeric G protein, the $G\beta\gamma$ subunit interacts with Switch II and the phosphate binding region, reducing the dynamics of this region. $G\beta\gamma$ binding significantly limits nucleotide exchange of the G protein in the absence of receptor (11, 28, 35). When the receptor interacts with the heterotrimeric G protein, it rotates the $\alpha 5$ helix and initiates the nucleotide release mechanism.

The Ins4A mutant shows similar receptor binding capability compared with WT protein. The nucleotide binding and release data show that the Ala insertion significantly affects the G protein nucleotide interaction. The heterotrimeric Ins4A mutant releases GDP almost 100-fold more slowly than WT in the presence of activated receptor. Comparison with the $GTP\gamma S$ binding kinetics allows us to conclude that GDP release is the main affected event. However, even with a very slow nucleotide exchange rate, $GTP\gamma S$ can still access the nucleotide binding pocket. However, release from the receptor-G protein complex is abolished even in the presence of high concentrations of either GDP or $GTP\gamma S$. This indicates that disrupting the hydrophobic core not only affects nucleotide interaction with the $G\alpha$ subunit in the receptor G protein complex but also that the G protein can no longer release from the receptor complex.

How does the heterotrimeric G protein bind normally to the receptor and interact with the nucleotide but not release from the receptor complex? The $\beta 6$ - $\alpha 5$ loop directly interacts with the guanine ring of the nucleotide, and it is the only direct way to connect the nucleotide binding region to the receptor through the $\alpha 5$ helix. Within the $\beta 6$ - $\alpha 5$ loop resides a conserved TCAT motif that mediates key contacts with the guanine ring of GDP that are believed to stabilize the binding of GDP within $G\alpha$. Indeed, mutations within this region result in enhanced spontaneous nucleotide exchange rates (36–38).

Thus, receptor contacts to the $G\alpha$ C terminus communicate structural changes through the $\alpha 5$ helix, which may modulate the conformation of the $\beta 6$ - $\alpha 5$ loop, ultimately resulting in the release of GDP. The N terminus of the $\alpha 5$ helix is unfolded in the $\beta 2AR$ -Gs complex structure (8). Recently, Dror *et al.* suggested that the structural rearrangements in the $\beta 6$ - $\alpha 5$ loop are the key events in G protein activation and GDP release (21). To examine environmental changes around this region, we fluorescently labeled residues Leu²⁷³ (αG) and K330 ($\alpha 5$) and showed that the N terminus of the $\alpha 5$ helix does not properly refold in the presence of nucleotide. This result indicates that either the 4-alanine insertion creates a buffer due to the extra length of the $\alpha 5$ helix between the receptor and nucleotide binding site of $G\alpha$ subunit, or it disturbs the nucleotide-dependent rearrangement of the N terminus of the $\alpha 5$ helix (residues 368–371 in $G\alpha_s$ and 328–331 in $G\alpha_{i1}$).

To address the question of whether slow nucleotide exchange and receptor release are caused by the increased length of the C-terminal helix, the repeated set of 4 WT amino acid residues was inserted back into the same region (Ins4X; Fig. 1B). This restores the hydrophobic core around Phe³³⁶ ($\alpha 5$) while maintaining the longer $\alpha 5$ helix. Notably, Ins4X showed similar basal and receptor-mediated nucleotide exchange activ-

ity to WT. In addition, it recovered its receptor release activity after guanine nucleotide incubation. This is consistent with previous studies (9, 31); Natochin *et al.* (31) showed that an 11-amino acid insertion above the hydrophobic core region (between Ile³⁴³ and Ile³⁴⁴) did not affect G protein-receptor binding and G protein activation compared with the WT protein. This indicates that it is not the length of the C terminus but rather maintaining the hydrophobic core interactions that is critical to complete the receptor-mediated G protein activation cycle.

In summary, the Ins4A crystal structure showed how $\alpha 5$ rotation significantly changes the conformation of $\beta 2$ - $\beta 3$ and the $\alpha 1$ helix. Phe³³⁶ is probably making direct hydrophobic contacts with Phe¹⁹¹ and Met⁵³, and it may also communicate with Phe¹⁸⁹ indirectly. Residues Met⁵³-His⁵⁷-Phe¹⁹¹ interact with Phe¹⁸⁹ through a π - π interaction between residues His⁵⁷ and Phe¹⁸⁹. In addition, Gln⁵², Ile⁵⁵, and Ile⁵⁶ in the $\alpha 1$ helix also interact with Thr³²⁹ and Gln³³³ in the $\alpha 5$ helix.

This network not only plays a major role during G protein activation, but it also influences proper rearrangement of the N terminus of the $\alpha 5$ helix to allow release of $G\alpha$ from the activated receptor after nucleotide binding. Thus, this study highlights changes through the G protein for receptor-mediated GDP release and G protein activation but also the reverse communication from GDP binding to release of the G protein from the activated receptor. How G proteins influence the ligand binding of receptor, leading to a high affinity ligand binding and, in the case of rhodopsin, Meta II stabilization, is currently unknown. This study provides the first clue that rearrangement of the N terminus of the $\alpha 5$ helix and re-engagement of the hydrophobic core are important elements of that signaling back to the receptor.

This mechanism might be generalizable for many receptor-G protein combinations; indeed, all residues of this hydrophobic core and the N terminus of the $\alpha 5$ helix are highly conserved in heterotrimeric G proteins. Our results support and experimentally demonstrate that the structural rearrangements of this region complete the G protein activation cycle. Although different receptor-mediated G protein activation models are presented as opposing mechanisms (4, 7, 9, 11, 20, 21, 27, 39), they may play complementary roles in the overall action of activated receptors. However, further studies are needed to identify the sequence of events involved in receptor-mediated G protein activation in molecular detail.

Experimental Procedures

Materials—The TSKgel G2000SW and G3000SW columns, GDP, and $GTP\gamma S$ were purchased from Sigma. BODIPY-GDP and - $GTP\gamma S$ were purchased from Thermo Fisher Scientific. All other reagents and chemicals were of the highest available purity.

Construction, Expression, and Purification of Proteins—In this study, recombinant $G\alpha_{i1}$ was used for all experiments instead of visual $G\alpha$ protein ($G\alpha_t$), given that $G\alpha_i$ is a very close homolog of $G\alpha_t$ yet is more easily expressed in *E. coli*. Briefly, the pSV277 expression vector encoding $G\alpha_{i1}$ with an N-terminal His tag served as the template for introducing amino acid insertions between residues Gln³³³ and Phe³³⁴ by using the

QuikChange system (Stratagene). The 4-Ala insertion (Ins4A- $G\alpha_{i1}$) mutant used primers 5'-GTA ACG GAC GTC ATC GCA GCA GCA GCA ATA AAG AAT AAC C-3' (forward) and 5'-G GTT ATT CTT TAT TGC TGC TGC TGC GAT GAC GTC CGT TAC-3' (reverse). The Phe-Val-Phe-Asp insertion (Ins4X- $G\alpha_{i1}$) mutant used primers 5'-CG AAG AAT GTG CAG TTT GTG TTC GAT TTT GTG TTC GAT GC-3' (forward) and 5'-GC ATC GAA CAC AAA ATC GAA CAC AAA CTG CAC ATT CTT CG-3' (reverse). All mutations were confirmed by DNA sequencing (GenHunter Corp.). The WT and the mutant constructs were expressed and purified as described previously (22). The purified proteins were cleaved with thrombin (Sigma; 0.5 units/mg final concentration) for 16 h at 4 °C to remove the N-terminal His tag. The samples were then loaded onto a nickel-nitrilotriacetic acid column to separate the proteins from the cleaved His tag and any uncleaved fraction. For further purification, the protein solutions were loaded onto a size exclusion chromatography column (TSKgel G3000SW) that was equilibrated in buffer A (50 mM Tris-HCl (pH 7.4), 100 mM NaCl, 1 mM $MgCl_2$, 20 μ M GDP (or 1 μ M GTP γ S), 1 mM DTT, and 100 μ M PMSE). SDS-PAGE was used to test the purity of the proteins. Urea-washed ROS membranes containing dark-adapted rhodopsin and $G\beta_1\gamma_1$ subunits were prepared as described previously (40, 41). Protein concentrations were determined spectroscopically (41) and by a Bradford assay (42).

Preparation of Urea-washed ROS Membranes and $G\beta_1\gamma_1$ —Urea-washed ROS membranes and $G\beta_1\gamma_1$ were prepared from bovine retina as described previously (40, 43).

Nucleotide Exchange Assays—The basal rate of GTP γ S binding was determined by monitoring the relative increase in the intrinsic tryptophan (Trp²¹¹) fluorescence ($\lambda_{ex} = 290$ nm, $\lambda_{em} = 340$ nm) of $G\alpha_{i1}$ (200 nM) in buffer containing 50 mM Tris (pH 7.2), 100 mM NaCl, and 1 mM $MgCl_2$ for at least 60 min at 21 °C after the addition of 10 μ M GTP γ S. Receptor-mediated nucleotide exchange was determined with $G\beta_1\gamma_1$ (400 nM) in the presence of 50 nM rhodopsin at 21 °C for 60 min after the addition of GTP γ S. The data were normalized to the baseline and maximum fluorescence and then fit to the exponential association equation ($y = y_{max} \times (1 - e^{-kt})$) to calculate the rate constant (k) as described previously (44). For nucleotide exchange experiments with BODIPY nucleotides, the fluorophore was monitored at $\lambda_{ex} = 490$ nm and $\lambda_{em} = 510$ nm with 5-nm slit widths as described (45). All experiments were performed in a buffer containing 50 mM Tris (pH 7.2), 100 mM NaCl, 1 mM $MgCl_2$, and 1 mM DTT at 21 °C. To measure the GDP release from the G protein, the $G\alpha_{i1}$ subunit was incubated with BODIPY-GDP in the absence of unlabeled GDP, $G\beta\gamma$ subunit, or receptor for 90 min at room temperature to exchange GDP with BODIPY nucleotide. After 1.5 h, a 2-fold excess of $G\beta\gamma$ was added and incubated for 15 min to suppress the nucleotide exchange. BODIPY-GDP-bound heterotrimeric G protein was recorded as the basal signal. After 2.5 min, light-activated receptor was added to the quartz cuvette. To measure the BODIPY-GTP γ S binding, heterotrimeric G proteins were incubated in buffer containing 50 mM Tris (pH 7.2), 100 mM NaCl, and 1 mM $MgCl_2$ in the presence of labeled GTP γ S to obtain the basal signal; after 2.5 min, activated receptor was added to initiate the exchange reaction. The kinetic data were

plotted and fit to a one-phase association function. Data represent the averages from 8–10 experiments.

Protein Labeling—A cysteine-reduced $G\alpha_{i1}$ protein (C3S, C66A, C214S, C305S, C325I, C351I) was labeled as described previously using a 10-fold molar excess of Alexa Fluor 594C5-maleimide (A1) (Invitrogen), with a labeling time of 3–5 h in 50 mM Tris (pH 7.5), 100 mM NaCl, 1 mM $MgCl_2$, and 20 μ M GDP (44). Proteins were purified via size exclusion purification, and the fractions were screened by intrinsic Trp fluorescence to ensure the functional integrity of the labeled proteins. Labeling efficiency was determined from comparison of A_{580} with protein concentration, as determined by Bradford, and found to be between 0.5 and 0.75 mol of label/mol of protein, depending on the location of the residue (44, 45).

Membrane Binding Assay—The ability of mutant $G\alpha_{i1}$ subunits to bind R^* in urea-washed ROS membranes was determined as described previously (7). Each sample was evaluated by comparison of the amount of $G\alpha_{i1}$ subunit within the pellet (P) or supernatant (S) with the total amount of $G\alpha_{i1}$ subunit (P + S) in both treatments expressed as a percentage of the total $G\alpha_{i1}$ protein. Data represent the average of at least five experiments.

Protein Crystallization, Data Collection, and Structure Determination—Purified GTP γ S-bound Ins4A- $G\alpha_{i1}$ subunits were exchanged into crystallization buffer (50 mM HEPES (pH 8.0), 1 mM EDTA, 10 mM $MgSO_4$, 5 mM DTT, 20 μ M GTP γ S) using a TSKgel G3000SW size exclusion chromatography column. Appropriate fractions were pooled as described above, and SDS-PAGE was used to assess the purity of the proteins. Crystals were grown using the hanging drop vapor diffusion method at 21 °C by equilibrating a 1:1 ratio of protein (10 mg/ml in crystallization buffer) and reservoir solution (12–16% PEG 2000 monomethyl ether, 18% 2-propanol, and 100 mM MES (pH 6.0)) against a reservoir solution. Crystals appeared after 15 days and grew in the primitive monoclinic space group $P2_1$.

For Ins4A- $G\alpha_{i1}\beta_1\gamma_1$ crystallization, separately purified and concentrated Ins4A- $G\alpha_{i1}$ and WT $G\beta_1\gamma_1$ subunits were mixed in a 1:1 molar ratio and incubated for 30 min at 25 °C. The heterotrimeric G protein complex was purified away from uncomplexed subunits using a G3000SW size exclusion chromatography column equilibrated with buffer containing 20 mM HEPES (pH 7.5), 150 mM NaCl, 1 mM EDTA, 5 mM DTT, and 200 μ M GDP. Appropriate fractions were pooled, and the post-translational palmitoylation of the $G\beta_1\gamma_1$ subunit was removed by incubating with 10 units of endoproteinase Lys-C in 50 mM Tris (pH 7.5; 150 mM NaCl) for 24 h at 4 °C (25). The protein complex was subjected to an additional step of size exclusion chromatography using a G3000SW column, as described above. Fractions were analyzed by SDS-PAGE to provide a guide to appropriate pooling of the purified heterotrimer. Heterotrimeric complex was crystallized using the hanging drop vapor diffusion method at 21 °C by equilibrating the protein (10 mg/ml in 20 mM HEPES (pH 7.5), 150 mM NaCl, 200 μ M GDP, 1 mM EDTA) in a 1:1 ratio with reservoir solution against a reservoir solution containing 19–24% PEG 8000, 1–5% 2-propanol, 1% n-octyl- β -D-glucopyranoside, 100 mM HEPES (pH

Structure of a G α C-terminal Insertion Mutant

7.0), and 100 mM NaOAc (pH 6.4). Crystals appeared after 5 days and grew in the primitive tetragonal space group P4₃.

Both Ins4A-G α_{i1} -GTP γ S and Ins4A-G $\alpha_{i1}\beta_1\gamma_1$ crystals were cryo-protected prior to data collection by briefly soaking in stabilization solution containing 18% glycerol and cryo-cooled by plunging into liquid nitrogen. Data sets were collected at the Life Sciences Collaborative Access Team (21-ID-G) of the Advanced Photon Source at Argonne National Laboratory at -180°C using a wavelength of 0.98 Å on a MAR CCD detector. Data were scaled using HKL2000 (46), truncated and converted using CCP4 (47), and processed using Phenix suites (48). Crystallographic data collection and refinement statistics are reported in Table 2. Criteria for data cutoffs were a combination of R_{sym} and I/σ , which both rose to unacceptable levels if the resolution were extended for either data set. The structures of Ins4A-G α_{i1} -GTP γ S·Mg²⁺ and Ins4A-G $\alpha_{i1}\beta_1\gamma_1$ -GDP complexes were determined by molecular replacement using 1GIA (WT G α_{i1} -GTP γ S·Mg²⁺) (26) and 1GP2 (WT G $\alpha_{i1}\beta_1\gamma_2$ -GDP) (24) as search models for Phaser-MR (49) in the Phenix suite (48). Because PDB entries 1GIA and 1GP2 were deposited prior to the requirement for deposition of structural factors, R-free reflections were randomly selected for Ins4A-G α_{i1} -GTP γ S·Mg²⁺ and Ins4A-G $\alpha_{i1}\beta_1\gamma_1$ -GDP. As a result, the free-R is of limited utility. Model building was performed in Coot (50) using composite omit maps calculated in Phenix (48) to minimize model bias. Refinement was conducted using both Refmac (51) and Phenix (48), with the final rounds of refinement performed using Phenix (48). In the final model, the regions corresponding to amino acids 1–33 and 348–354 (corresponding to WT numbers) in Ins4A-G α_{i1} -GTP γ S·Mg²⁺ are not included. Similarly, in the Ins4A-G $\alpha_{i1}\beta_1\gamma_1$ -GDP structure, residue numbers 1–6 and 346–354 in the G α_{i1} subunit, 1 and 129–132 in the G β_1 subunit, and 1–9 and 66–74 in the G γ_1 subunit are not included due to the lack of interpretable electron density. Structural superimpositions were performed using C α atoms and the program Superpose in the CCP4 suite (52, 53). All structural figures were made using PyMOL (PyMOL Molecular Graphics System version 1.5.0.4, Schrödinger, LLC, New York) unless otherwise indicated.

Rosetta Interface Energy Calculations—Interface energies were computed following the Rosetta $\Delta\Delta G$ protocol described previously (54, 55). Briefly, we re-relaxed the previously published ensembles of 10 structures of the G protein in the basal state and receptor-bound state using a DualSpace relax Rosetta protocol (56) for consistency between the mutant structures and the *in silico* models (55). The G γ subunit of the receptor-bound models was truncated along both the N and C termini to match the available crystal density of the mutant structures. For the Ins4A insertion protein, all residues present with crystallographic density were included in the analyses. The Ins4A-G α_{i1} and Ins4A-G $\alpha_{i1}\beta_1\gamma_1$ structures were relaxed using the same DualSpace relax protocol in Rosetta. Residue-residue interactions across the $\alpha 1$ helix/GTPase domain interface were evaluated by measuring the changes in energetic perturbations when computationally removing the $\alpha 1$ helices from the models. The $\alpha 1$ helix was defined as residues Gly⁴⁵–Glu⁵⁸. For all analyses, GDP·Mg²⁺ or GTP γ S remained positioned within the nucleotide binding pocket. The predicted $\Delta\Delta G$ value is reported as an

average over the 10 best structural models in REUs. Absolute values >0.5 REUs are considered to be significant. Using the S.D. values over the 10 structures, a Z-score was computed. The total $\Delta\Delta G$ value across the interface is calculated as the sum of individual residue contributions.

Rosetta Pairwise Interaction Score Calculations—Average interaction scores between pairwise interacting residues were computed using Rosetta's per residue energy breakdown protocol as described previously (55). The strength between all possible pairs of interacting amino acid residues within the G protein were calculated across the previously published ensembles of 10 structures after an initial energy minimization using the DualSpace relaxation protocol (56). Mutant crystal structures of Ins4A-G α_{i1} and Ins4A-G $\alpha_{i1}\beta_1\gamma_1$ also underwent an initial round of DualSpace relax using Rosetta to relieve minor energetic clashes, in both torsional and Cartesian space, induced by crystallization before calculations were conducted. The resulting predicted interaction scores, between all residue pairs, was then averaged across the top 10 scoring models (as assessed by total Rosetta energy) in the basal state, receptor-bound state, and activated monomeric state. Predicted values are reported in REUs and considered significant if >0.5 REUs. Although these scores are also reported in REUs, they are *not* free energies in the thermodynamic sense. We therefore call these values pairwise "interaction scores" for intramolecular probing of information flow.

Author Contributions—A. I. K. prepared mutant constructs, expressed and purified G protein α subunit and purified heterotrimeric G protein for both biochemical assays and crystallization, performed protein labeling, performed all biochemical assays and analyzed results, performed crystallization trials, optimized crystallization conditions, collected diffraction data, solved and refined the structures, and wrote the manuscript. A. D. L. performed and analyzed Rosetta energy and pairwise interaction calculations and wrote the manuscript with A. I. K. J. A. G. assisted with protein expression and purification of G $\beta\gamma$ subunit. T. M. I. supervised the x-ray diffraction data processing and crystal structure refinement and wrote the manuscript with A. I. K. J. M. supervised Rosetta energy and pairwise interaction calculations and assisted with manuscript preparation. H. E. H. initiated and planned the project, supervised the research, and wrote the manuscript with A. I. K.

Acknowledgments—We thank Jin Liao for excellent technical assistance. A portion of the experiments described here used the Vanderbilt PacVan robotic crystallization facility, which was supported by National Institutes of Health Grant S10 RR026915. Use of the Advanced Photon Source, an Office of Science User Facility operated for the United States Department of Energy Office of Science by Argonne National Laboratory, was supported by the United States Department of Energy under Contract DE-AC02-06CH11357. Use of the Life Sciences Collaborative Access Team Sector 21 was supported by the Michigan Economic Development Corporation and the Michigan Technology Tri-Corridor (Grant 085P1000817).

References

1. Oldham, W. M., and Hamm, H. E. (2007) How do receptors activate G proteins? *Adv. Protein Chem.* **74**, 67–93

2. Sprang, S. R. (1997) G Protein Mechanisms: insights from structural analysis. *Annu. Rev. Biochem.* **66**, 639–678
3. Higashijima, T., Ferguson, K. M., Smigel, M. D., and Gilman, A. G. (1987) The effect of GTP and Mg²⁺ on the GTPase activity and the fluorescent properties of G_o. *J. Biol. Chem.* **262**, 757–761
4. Onrust, R., Herzmark, P., Chi, P., Garcia, P. D., Lichtarge, O., Kingsley, C., and Bourne, H. R. (1997) Receptor and $\beta\gamma$ binding sites in the α subunit of the retinal G protein transducin. *Science* **275**, 381–384
5. Johnston, C. A., and Siderovski, D. P. (2007) Receptor-mediated activation of heterotrimeric G-proteins: current structural insights. *Mol. Pharmacol.* **72**, 219–230
6. Kimple, A. J., Bosch, D. E., Giguère, P. M., and Siderovski, D. P. (2011) Regulators of G-protein signaling and their G α substrates: promises and challenges in their use as drug discovery targets. *Pharmacol. Rev.* **63**, 728–749
7. Oldham, W. M., Van Eps, N., Preininger, A. M., Hubbell, W. L., and Hamm, H. E. (2006) Mechanism of the receptor-catalyzed activation of heterotrimeric G proteins. *Nat. Struct. Mol. Biol.* **13**, 772–777
8. Rasmussen, S. G., DeVree, B. T., Zou, Y., Kruse, A. C., Chung, K. Y., Kobilka, T. S., Thian, F. S., Chae, P. S., Pardon, E., Calinski, D., Mathiesen, J. M., Shah, S. T., Lyons, J. A., Caffrey, M., Gellman, S. H., et al. (2011) Crystal structure of the β_2 -adrenergic receptor-G_s protein complex. *Nature* **477**, 549–555
9. Marin, E. P., Krishna, A. G., and Sakmar, T. P. (2002) Disruption of the $\alpha 5$ helix of transducin impairs rhodopsin-catalyzed nucleotide exchange. *Biochemistry* **41**, 6988–6994
10. Ceruso, M. A., Periole, X., and Weinstein, H. (2004) Molecular dynamics simulations of transducin: interdomain and front to back communication in activation and nucleotide exchange. *J. Mol. Biol.* **338**, 469–481
11. Kaya, A. I., Lokits, A. D., Gilbert, J. A., Iverson, T. M., Meiler, J., and Hamm, H. E. (2014) A conserved phenylalanine as a relay between the $\alpha 5$ helix and the GDP binding region of heterotrimeric G_i protein α subunit. *J. Biol. Chem.* **289**, 24475–24487
12. Valencia, A., Chardin, P., Wittinghofer, A., and Sander, C. (1991) The Ras protein family: evolutionary tree and role of conserved amino acids. *Biochemistry* **30**, 4637–4648
13. Quilliam, L. A., Zhong, S., Rabun, K. M., Carpenter, J. W., South, T. L., Der, C. J., and Campbell-Burk, S. (1995) Biological and structural characterization of a Ras transforming mutation at the phenylalanine-156 residue, which is conserved in all members of the Ras superfamily. *Proc. Natl. Acad. Sci. U.S.A.* **92**, 1272–1276
14. Wilkie, T. M., Gilbert, D. J., Olsen, A. S., Chen, X. N., Amatruda, T. T., Korenberg, J. R., Trask, B. J., de Jong, P., Reed, R. R., and Simon, M. I. (1992) Evolution of the mammalian G protein alpha subunit multigene family. *Nat. Genet.* **1**, 85–91
15. Johnston, C. A., Willard, M. D., Kimple, A. J., Siderovski, D. P., and Willard, F. S. (2008) A sweet cycle for *Arabidopsis* G-proteins: recent discoveries and controversies in plant G-protein signal transduction. *Plant Signal. Behav.* **3**, 1067–1076
16. Jones, J. C., Duffy, J. W., Machius, M., Temple, B. R., Dohlman, H. G., and Jones, A. M. (2011) The crystal structure of a self-activating G protein α subunit reveals its distinct mechanism of signal initiation. *Sci. Signal.* **4**, ra8
17. Bradford, W., Buckholz, A., Morton, J., Price, C., Jones, A. M., and Urano, D. (2013) Eukaryotic G protein signaling evolved to require G protein-coupled receptors for activation. *Sci. Signal.* **6**, ra37
18. Ma, H., Yanofsky, M. F., and Meyerowitz, E. M. (1990) Molecular cloning and characterization of GPA1, a G protein α subunit gene from *Arabidopsis thaliana*. *Proc. Natl. Acad. Sci. U.S.A.* **87**, 3821–3825
19. Alexander, N. S., Preininger, A. M., Kaya, A. I., Stein, R. A., Hamm, H. E., and Meiler, J. (2014) Energetic analysis of the rhodopsin-G-protein complex links the $\alpha 5$ helix to GDP release. *Nat. Struct. Mol. Biol.* **21**, 56–63
20. Flock, T., Ravarani, C. N., Sun, D., Venkatakrishnan, A. J., Kayikci, M., Tate, C. G., Veprintsev, D. B., and Babu, M. M. (2015) Universal allosteric mechanism for G α activation by GPCRs. *Nature* **524**, 173–179
21. Dror, R. O., Mildorf, T. J., Hilger, D., Manglik, A., Borhani, D. W., Arlow, D. H., Philippsen, A., Villanueva, N., Yang, Z., Lerch, M. T., Hubbell, W. L., Kobilka, B. K., Sunahara, R. K., and Shaw, D. E. (2015) Signal Transduction: structural basis for nucleotide exchange in heterotrimeric G proteins. *Science* **348**, 1361–1365
22. Medkova, M., Preininger, A. M., Yu, N. J., Hubbell, W. L., and Hamm, H. E. (2002) Conformational changes in the amino-terminal helix of the G protein α_1 following dissociation from G $\beta\gamma$ subunit and activation. *Biochemistry* **41**, 9962–9972
23. Coleman, D. E., and Sprang, S. R. (1998) Crystal structures of the G protein G_{ia1} complexed with GDP and Mg²⁺: a crystallographic titration experiment. *Biochemistry* **37**, 14376–14385
24. Wall, M. A., Coleman, D. E., Lee, E., Iñiguez-Lluhi, J. A., Posner, B. A., Gilman, A. G., and Sprang, S. R. (1995) The structure of the G protein heterotrimer G_{ia1} $\beta_1\gamma_2$. *Cell* **83**, 1047–1058
25. Lambright, D. G., Sondek, J., Bohm, A., Skiba, N. P., Hamm, H. E., and Sigler, P. B. (1996) The 2.0 Å crystal structure of a heterotrimeric G protein. *Nature* **379**, 311–319
26. Coleman, D. E., Berghuis, A. M., Lee, E., Linder, M. E., Gilman, A. G., and Sprang, S. R. (1994) Structures of active conformations of G_{ia1} and the mechanism of GTP hydrolysis. *Science* **265**, 1405–1412
27. Sun, D., Flock, T., Deupi, X., Maeda, S., Matkovic, M., Mendieta, S., Mayer, D., Dawson, R. J., Schertler, G. F., Babu, M. M., and Veprintsev, D. B. (2015) Probing G α i1 protein activation at single-amino acid resolution. *Nat. Struct. Mol. Biol.* **22**, 686–694
28. Kapoor, N., Menon, S. T., Chauhan, R., Sachdev, P., and Sakmar, T. P. (2009) Structural evidence for a sequential release mechanism for activation of heterotrimeric G proteins. *J. Mol. Biol.* **393**, 882–897
29. Bourne, H. R. (1997) How receptors talk to trimeric G proteins. *Curr. Opin. Cell Biol.* **9**, 134–142
30. Rondard, P., Iiri, T., Srinivasan, S., Meng, E., Fujita, T., and Bourne, H. R. (2001) Mutant G protein α subunit activated by G $\beta\gamma$: a model for receptor activation? *Proc. Natl. Acad. Sci. U.S.A.* **98**, 6150–6155
31. Natchin, M., Moussaif, M., and Artemyev, N. O. (2001) Probing the mechanism of rhodopsin-catalyzed transducin activation. *J. Neurochem.* **77**, 202–210
32. Oldham, W. M., and Hamm, H. E. (2006) Structural basis of function in heterotrimeric G proteins. *Q. Rev. Biophys.* **39**, 117–166
33. Oldham, W. M., and Hamm, H. E. (2008) Heterotrimeric G protein activation by G-protein-coupled receptors. *Nat. Rev. Mol. Cell Biol.* **9**, 60–71
34. Chung, K. Y., Rasmussen, S. G., Liu, T., Li, S., DeVree, B. T., Chae, P. S., Calinski, D., Kobilka, B. K., Woods, V. L., Jr., and Sunahara, R. K. (2011) Conformational changes in the G protein G_s induced by the β_2 -adrenergic receptor. *Nature* **477**, 611–615
35. Higashijima, T., Ferguson, K. M., Sternweis, P. C., Smigel, M. D., and Gilman, A. G. (1987) Effects of Mg²⁺ and the $\beta\gamma$ -subunit complex on the interactions of guanine nucleotides with G proteins. *J. Biol. Chem.* **262**, 762–766
36. Thomas, T. C., Schmidt, C. J., and Neer, E. J. (1993) G-protein α_o subunit: mutation of conserved cysteines identifies a subunit contact surface and alters GDP affinity. *Proc. Natl. Acad. Sci. U.S.A.* **90**, 10295–10299
37. Iiri, T., Herzmark, P., Nakamoto, J. M., van Dop, C., and Bourne, H. R. (1994) Rapid GDP release from G_{sa} in patients with gain and loss of endocrine function. *Nature* **371**, 164–168
38. Posner, B. A., Mixon, M. B., Wall, M. A., Sprang, S. R., and Gilman, A. G. (1998) The A326S mutant of G_{ia1} as an approximation of the receptor-bound state. *J. Biol. Chem.* **273**, 21752–21758
39. Cherfils, J., and Chabre, M. (2003) Activation of G-protein G α subunits by receptors through G α -G β and G α -G γ interactions. *Trends Biochem. Sci.* **28**, 13–17
40. Mazzoni, M. R., Malinski, J. A., and Hamm, H. E. (1991) Structural analysis of rod GTP-binding protein, G_i: limited proteolytic digestion pattern of G_i with four proteases defines monoclonal antibody epitope. *J. Biol. Chem.* **266**, 14072–14081
41. Kaya, A. I., Thaker, T. M., Preininger, A. M., Iverson, T. M., and Hamm, H. E. (2011) Coupling efficiency of rhodopsin and transducin in bicelles. *Biochemistry* **50**, 3193–3203
42. Bradford, M. M. (1976) A rapid and sensitive method for the quantitation of microgram quantities of protein utilizing the principle of protein-dye binding. *Anal. Biochem.* **72**, 248–254
43. Thaker, T. M., Kaya, A. I., Preininger, A. M., Hamm, H. E., and Iverson,

Structure of a G α C-terminal Insertion Mutant

- T. M. (2012) Allosteric mechanisms of G protein-coupled receptor signaling: a structural perspective. *Methods Mol. Biol.* **796**, 133–174
44. Preininger, A. M., Kaya, A. I., Gilbert, J. A., 3rd, Busenlehner, L. S., Armstrong, R. N., and Hamm, H. E. (2012) Myristoylation exerts direct and allosteric effects on G α conformation and dynamics in solution. *Biochemistry* **51**, 1911–1924
45. Hamm, H. E., Kaya, A. I., Gilbert, J. A., 3rd, and Preininger, A. M. (2013) Linking receptor activation to changes in Sw I and II of G α proteins. *J. Struct. Biol.* **184**, 63–74
46. Otwinowski, Z., and Minor, W. (1997) Processing of x-ray diffraction data collected in oscillation mode. *Methods Enzymol.* **276**, 307–326
47. Potterton, E., Briggs, P., Turkenburg, M., and Dodson, E. (2003) A graphical user interface to the CCP4 program suite. *Acta Crystallogr. D Biol. Crystallogr.* **59**, 1131–1137
48. Adams, P. D., Afonine, P. V., Bunkóczi, G., Chen, V. B., Davis, I. W., Echols, N., Headd, J. J., Hung L.-W., Kapral, G. J., Grosse-Kunstleve, R. W., McCoy, A. J., Moriarty, N. W., Oeffner, R., Read, R. J., Richardson, D. C., *et al.* (2010) PHENIX: a comprehensive Python-based system for macromolecular structure solution. *Acta Crystallogr. D Biol. Crystallogr.* **66**, 213–221
49. McCoy, A. J., Grosse-Kunstleve, R. W., Adams, P. D., Winn, M. D., Storoni, L. C., and Read, R. J. (2007) Phaser crystallographic software. *J. Appl. Crystallogr.* **40**, 658–674
50. Emsley, P., and Cowtan, K. (2004) Coot: model-building tools for molecular graphics. *Acta Crystallogr. D Biol. Crystallogr.* **60**, 2126–2132
51. Murshudov, G. N., Vagin, A. A., and Dodson, E. J. (1997) Refinement of macromolecular structures by the maximum-likelihood method. *Acta Crystallogr. D Biol. Crystallogr.* **53**, 240–255
52. Winn, M. D., Ballard, C. C., Cowtan, K. D., Dodson, E. J., Emsley, P., Evans, P. R., Keegan, R. M., Krissinel, E. B., Leslie, A. G., McCoy, A., McNicholas, S. J., Murshudov, G. N., Pannu, N. S., Potterton, E. A., Powell, H. R., *et al.* (2011) Overview of the CCP4 suite and current developments. *Acta Crystallogr. D Biol. Crystallogr.* **67**, 235–242
53. Krissinel, E., and Henrick, K. (2004) Secondary-structure matching (SSM), a new tool for fast protein structure alignment in three dimensions. *Acta Crystallogr. D Biol. Crystallogr.* **60**, 2256–2268
54. Kellogg, E. H., Leaver-Fay, A., and Baker, D. (2011) Role of conformational sampling in computing mutation-induced changes in protein structure and stability. *Proteins* **79**, 830–838
55. Lokits, A. D., Leman, J. K., Kitko, K. E., Alexander, N. S., Hamm, H. E., and Meiler, J. (2015) A survey of conformational and energetic changes in G protein signaling. *AIMS Biophys.* **2**, 630–648
56. Conway, P., Tyka, M. D., DiMaio, F., Konerding, D. E., and Baker, D. (2014) Relaxation of backbone bond geometry improves protein energy landscape modeling. *Protein Sci.* **23**, 47–55
57. Chen, V. B., Arendall, W. B., 3rd, Headd, J. J., Keedy, D. A., Immormino, R. M., Kapral, G. J., Murray, L. W., Richardson, J. S., and Richardson, D. C. (2010) MolProbity: all-atom structure validation for macromolecular crystallography. *Acta Crystallogr. D Biol. Crystallogr.* **66**, 12–21

A Conserved Hydrophobic Core in G α ₁ Regulates G Protein Activation and Release from Activated Receptor

Ali I. Kaya, Alyssa D. Lokits, James A. Gilbert, T. M. Iverson, Jens Meiler and Heidi E. Hamm

J. Biol. Chem. 2016, 291:19674-19686.

doi: 10.1074/jbc.M116.745513 originally published online July 26, 2016

Access the most updated version of this article at doi: [10.1074/jbc.M116.745513](https://doi.org/10.1074/jbc.M116.745513)

Alerts:

- [When this article is cited](#)
- [When a correction for this article is posted](#)

[Click here](#) to choose from all of JBC's e-mail alerts

This article cites 57 references, 16 of which can be accessed free at <http://www.jbc.org/content/291/37/19674.full.html#ref-list-1>